

Article

A Mechanistic Model on Catalyst Deactivation by Coke Formation in a CSTR Reactor

Ishaka Muhammad ^{1,2,*}, Nura Makwashi ³, Tariq Galadanchi Ahmed ⁴, George Manos ¹ and Donglin Zhao ^{5,*}

¹ Department of Chemical Engineering, University College London, London WC1E 7JE, UK; g.manos@ucl.ac.uk

² Department of Chemistry, Zamfara State College of Education, Maru, , Nigeria

³ Department of Chemical and Petroleum Engineering, Bayero University, Kano P.M.B 3011, Nigeria; nmakwashi.cpe@buk.edu.ng

⁴ School of Computing Engineering and Digital Technologies, Teesside University, Middlesbrough TS1 3BX, UK; t.ahmed@tees.ac.uk

⁵ School of Engineering, London South Bank University, London, SE1 0AA, UK

* Correspondence: ishakak2001@yahoo.com (I.M.); donglin.zhao@lsbu.ac.uk (D.Z.)

Abstract: A mechanistic model on catalyst deactivation by coke formation in a continuous stirred tank reactor (CSTR) has been developed in the paper. Catalyst deactivation by coke formation was treated as a surface reaction. Four reaction mechanisms representing coke formation through different routes were proposed. The evolved system of ordinary differential equations (ODEs) was solved numerically using MATLAB. This approach was validated by applying it to the skeletal isomerization of 1-pentene over ferrierite. Simulation results were compared qualitatively to those obtained from the literature. Simulation results indicated that coke formation is an extremely rapid process with fast formation of coke components on the strongest acid sites leading to final coke. The coke deposition is slower at higher residence times resulting in more stable product formation and weaker deactivation. The results obtained from this work revealed that the developed model is indeed able to successfully demonstrate the most essential features of catalyst deactivation by coke formation and are in agreement with the findings in the literature. Future work is aimed to extend the study to different reactors such as a plug flow reactor, in addition to analysis of the reaction system's sensitivity to variables such as temperature and pressure.

Citation: Muhammad, I.; Makwashi, N.; Ahmed, T.G.; Manos, G.; Zhao, D. A Mechanistic Model on Catalyst Deactivation by Coke Formation in a CSTR Reactor. *Processes* **2023**, *11*, x. <https://doi.org/10.3390/xxxxx>

Academic Editor(s): Vincenzo Russo, Pasi Tolvanen, Stefan Haase

Received: date

Revised: date

Accepted: date

Published: date



Copyright: © 2023 by the authors. Submitted for possible open access publication under the terms and conditions of the Creative Commons Attribution (CC BY) license (<https://creativecommons.org/licenses/by/4.0/>).

Keywords: mechanistic modelling; catalyst deactivation; coke formation; CSTR; catalytic cracking

1. Introduction

Catalytic cracking of hydrocarbons over zeolite-based catalysts is an important commercial process in refining and petrochemical industry, which suffers from strong coking within a few seconds [1,2] and causes an extremely fast catalyst deactivation [2,3]. Coke refers to a mixture of heavy, non-volatile reaction components that are strongly adsorbed on the surface of catalyst as a by-product, poisoning the active sites and/or blocking the catalyst pores [1–3]. The mechanism of coke formation is a complex process that involves the adsorption of coke precursors on the surface of the catalyst and their transformation inside the catalyst pores [2–4]. Coke precursors can be formed from the reactant molecules, reaction intermediates, product molecules and their combinations [4]. Pore blockage due to coke formation is a very common problem in zeolites catalysis. This restricts access of reactant molecules to the catalyst active sites [3,4]. The strength of the acid sites and higher acidity are among the main factors that determine the severity of coke formation [4,5]. Coking therefore usually affects the catalyst selection, reactor design and operation [5], and hence the design of catalytic cracking processes [6,7]. The rate of coke

formation and nature of its components are affected by the feedstock types, catalyst properties and operation conditions [3,8]. It has been reported [3,9] that the interaction between intermediates participating in coke formation and other reaction intermediates influence the final products distribution and products selectivity. Strong acid sites are more prone to coke deposition than weak acid sites, and therefore coke deposition is faster on strong acid sites [10–12]. Recently, more and more renewable feedstock has been used to produce fuels and chemicals. The molecules originating from renewable sources are more complex and they lead to more severe and complicated catalyst deactivation [5].

Researchers have successfully employed both mathematical models and experimental studies to predict the efficiency and optimize the process parameters in catalytic cracking [13–18], representing an important scientific task in the field of catalytic processes [13]. The accurate prediction of coke formation is an indispensable part of sustainable catalytic process, and therefore formulation of a precise model for the process will serve as a powerful tool for designing and evaluating reactor performances [8,13]. A comprehensive model can provide an insight into the effects of various process parameters on catalyst activity, selectivity and stability, as well as a means of optimizing the life of the catalyst [19,20]. A rational model of coke formation should be based on the general principles of kinetics and reaction mechanism involved in the process. This includes the following steps:

- (i) Identifying the reaction steps;
- (ii) Assuming plausible mechanisms;
- (iii) Deriving the rate expressions.

In this case, the deactivation can be expressed as a function of the coke coverage on the catalyst surface, and it is implicitly dependent on time [5]. The description of the deactivation with mechanistic approach results in a dynamic reactor model [21]. A similar approach was used by Sandelin et al. [5,21] to model catalyst deactivation by incorporating coke formation among the other elementary steps proceeding on the catalyst surfaces based on the principle of mechanistic modelling.

Mechanistic modelling accounts for the detailed reaction network in catalytic cracking as its basis [8]. This involves the combination of adsorbates mass balances and rate equations, alongside the formulation of an overall catalytic site balance. It is the most desired form of kinetic modelling due to the inclusion of surface species concentrations. Mechanistic modelling avoids the use of any assumptions, such as the rate-determining step, quasi-steady-state approximation, most abundant surface intermediate, or nearly empty surface [22].

The aim of this work is to develop a mechanistic model of catalyst deactivation by coke formation, which will be implemented on a prototype and real catalytic reactions with the following objectives:

- (i) Develop a mathematical model for hydrocarbon catalytic reaction incorporating catalyst deactivation by coke formation applied on isothermal a continuous stirred-tank reactor (CSTR) in order to capture the effect of the fast deactivation on the dynamic behavior of a CSTR;
- (ii) Explore plausible deactivation mechanisms by coke formation;
- (iii) Compare rival deactivation mechanisms;
- (iv) Carry out parametric study on the reaction system's tendency to deactivation through coking.

2. Methodology

2.1. Basics of the Kinetics and Reaction Mechanism

A simple liquid-phase catalytic reaction ($R \rightarrow P$) has been chosen as the starting point of this modelling. Based on this reaction system, several mechanisms were assumed and discussed, considering plausible reaction steps leading to coke formation and deposition on active sites. Based on chemisorption process principles, coke formation may occur in a

considerable number of ways leading to different reaction mechanisms. Simplification of these mechanisms, based on pseudo-monomolecular principles, are necessary due to the complexities that arise because of coke formation. This work investigates four different reaction mechanisms of catalyst deactivation by coke formation, based on the number of active sites occupied. The total number of sites per unit area are assumed constant and are regarded as locations upon which species reside. The mechanisms can be summarized as follows:

2.1.1. Mechanism I: One Surface Species Coking, Irreversible Surface Reaction

For this coking mechanism, coke (CS) is formed by the adsorbed reactant molecule (RS). In this case both coking and surface reaction are irreversible. The adsorption of the reactant molecule at the catalyst site is the only reversible step. The detailed mechanism is stated below:



where, (R) stands for the reactant, (S) denotes a vacant site on the catalyst surface, (RS) is the adsorbed reactant, (P) is the product and (CS) is the site inactivated by carbonaceous deposit (coke). Finally, k_1, k_{-1}, k_2 , and k_c stand for the rate constants corresponding to the adsorption forward reaction, adsorption reverse reaction, desorption forward reaction and coking reaction, respectively.

2.1.2. Mechanism II: One Surface Species Coking, Reversible Surface Reaction

The reversible surface reaction step distinguishes mechanism II from mechanism I.

The reaction steps are the same as in mechanism I with the reaction (2) now transformed into (4).



where k_{-2} is the rate constant of the reverse surface reaction step.

2.1.3. Mechanism III: Two Surface Species

Irreversible coking in mechanism III involves additional surface species to produce coke. All the adsorbed surface species participated in the coke formation, as depicted through the following mechanisms in addition to equations (3) and (4).



As shown in mechanism III, elementary steps (1) and (3) are the same as in the previous mechanisms, and new steps for surface reactions and coking were added as indicated by reactions (4), (5) and (6). The adsorbed reactant (RS) is transformed to another surface species (PS) which desorbed to form the product. The rate constants for the product desorption reversible reaction step (5) are represented by k_3 and k_{-3} whereas k_{c2} is the rate constant for coking reaction (6).

2.1.4. Mechanism IV: Two Surface Species, Reversible Coking

Mechanism IV contained reversible coking step which represent its main difference with mechanism III. The previous mechanisms assumed coke is formed via irreversible surface adsorption. This would eventually lead to complete loss of activity after prolonged time on stream. Instead, catalyst retained some activity after long reaction time. The reversible mechanism is expected to account for this behavior. When the deactivation is reversible and coke is formed from one surface species, reaction (3) is reversed

2.2. CSTR Reactor Model

A gradient-less isothermal CSTR was employed in the model. Mechanistic modelling based on several elementary steps as used here would ensure quantitative interpretation of the results from transient experiments. The exclusion of steady-state multiplicity eliminates the presence of complexities and makes it essential to use models that incorporate the chemical processes occurring on the catalyst surface. The assumptions used are as follows:

- The uniformity of the catalyst surface is assumed with intermediate interactions taking place on the catalyst surface and the effects of mass and heat transfer are considered negligible;
- Constant temperature and pressure operational conditions are assumed;
- CSTR is considered to be operating in regime of intrinsic kinetics with reaction mixture assumed to be well agitated.

Considering the CSTR is well-agitated and operating in the regime of intrinsic kinetics, the material balances of the bulk components and surface species are written as follows:

$$\text{rate of accumulation of component } i = \text{inlet flowrate of component } i - \text{outlet flowrate of component } i + \text{rate of generation of component } i$$

For a component i , the mole balance can be written in the following way:

$$\frac{dn_i}{dt} = \dot{n}_{i,in} - \dot{n}_{i,out} + r_i \rho_B V_R \quad (7)$$

where $\dot{n}_{i,in}$ denotes the inlet flow-rate of component i , $\dot{n}_{i,out}$ is the outlet flow-rate of component i , r_i represents the net formation rate of component i , V_R stands for the total reactor volume, and ρ_B is the bulk density of the catalyst. The bulk density, ρ_B , is expressed as:

$$\rho_B = \rho_{cat}^* (1 - \varepsilon) \quad (8)$$

where ρ_{cat}^* represents the catalyst density and ε is the catalyst bed voidage. Therefore, incorporating Equation (9) into the mole balance equation, Equation (8) can be written as:

$$\frac{dC_i}{dt} = \varepsilon^{-1} \left(\frac{\dot{n}_{i,in} - \dot{n}_{i,out}}{V_R} + r_i \rho_{cat}^* (1 - \varepsilon) \right) \quad (9)$$

Since residence time τ , is given by:

$$\tau = \frac{V_R}{v} \quad (10)$$

The mole balance of the bulk components is obtained by substituting Equation (11) into Equation (10).

$$\frac{dC_i}{dt} = \varepsilon^{-1} \left(\frac{C_{i,in} - C_{i,out}}{\tau} + r_i \rho_{cat}^* (1 - \varepsilon) \right) \quad (11)$$

In order to account for the surface species, the mass balance equation is written as follows:

$$\frac{d\theta_j}{dt} = r_j \quad (12)$$

where θ_j is the fraction of the total number of sites occupied by component j .

2.3. Rate Expressions and Material Balance Derivation

The rate expressions for all elementary reactions are derived and stated below.

2.3.1. Mechanism I

For Mechanism I, the rate expressions are:

$$r_1 = k_1 C_R \theta_S \quad (13)$$

$$r_{-1} = k_{-1} \theta_{RS} \quad (14)$$

$$r_2 = k_2 \theta_{RS} \quad (15)$$

$$r_c = k_c \theta_{RS} \quad (16)$$

Combining the reactor balance Equation (12) and the rate Equations (14)–(17), the following equations are obtained for the reactant and products mole balances.

$$\frac{dC_R}{dt} = \varepsilon^{-1} \left(\frac{C_{R,in} - C_R}{\tau} + (-r_1 + r_{-1}) \rho_{cat}^* (1 - \varepsilon) \right) \quad (17)$$

$$\frac{dC_P}{dt} = \varepsilon^{-1} \left(\frac{C_{P,in} - C_P}{\tau} + r_2 \rho_{cat}^* (1 - \varepsilon) \right) \quad (18)$$

Introducing the symbol $\rho_{cat} = \rho_{cat}^* (1 - \varepsilon) / \varepsilon$, Equations (18) and (19) become:

$$\frac{dC_R}{dt} = \frac{C_{R0} - C_R}{\varepsilon \tau} + (-r_1 + r_{-1}) \rho_{cat} \quad (19)$$

$$\frac{dC_P}{dt} = -\frac{C_P}{\varepsilon \tau} + r_2 \rho_{cat} \quad (20)$$

ρ_{cat} is not the catalyst density, but simply a symbol incorporating the catalyst density and bed voidage as in the equation above.

Inserting the rate expressions into Equation (13), the mole balance equations for surface species is obtained.

$$\frac{d\theta_{RS}}{dt} = r_1 - r_{-1} - r_2 - r_c \quad (21)$$

$$\frac{d\theta_S}{dt} = -r_1 + r_{-1} + r_2 \quad (22)$$

$$\frac{d\theta_C}{dt} = r_1 r_c \quad (23)$$

Using dimensionless concentrations by dividing with $C_{R,in}$ and symbolised by the respective concentration symbol with a bar, Equations (20)–(23) become:

$$\frac{d\bar{C}_R}{dt} = \frac{1}{\varepsilon \tau} \left(1 - \bar{C}_R \right) - k_1 \bar{C}_R \theta_S \rho_{cat} + \frac{k_{-1} \theta_{RS} \rho_{cat}}{C_{R,in}} \quad (24)$$

$$\frac{d\bar{C}_P}{dt} = -\frac{\bar{C}_P}{\varepsilon \tau} + \frac{k_2 \theta_{RS} \rho_{cat}}{C_{R,in}} \quad (25)$$

$$\frac{d\theta_{RS}}{dt} = k_1 \underline{C}_R \theta_S C_{R,in} - (k_{-1} + k_2 + k_c) \theta_{RS} \quad (26)$$

$$\frac{d\theta_S}{dt} = -k_1 \underline{C}_R C_{R,in} \theta_S + (k_{-1} + k_2) \theta_{RS} \quad (27)$$

2.3.2. Mechanism II

The rate expressions and material balance equations for mechanisms II are the same as those for mechanism I except the elementary reactions for the surface reactions. The rate expression for the reverse reaction (4) is given by:

$$r_{-2} = k_{-2} \underline{C}_P \theta_S \quad (28)$$

Consequently, the material balance equations for C_P , θ_{RS} and θ_S are stated below:

$$\frac{dC_P}{dt} = -\frac{C_P}{\varepsilon\tau} + \frac{k_2 \theta_{RS} \rho_{cat}}{C_{R,in}} - k_{-2} \underline{C}_P \theta_S \rho_{cat} \quad (29)$$

$$\frac{d\theta_{RS}}{dt} = k_1 \underline{C}_R \theta_S C_{R,in} - (k_{-1} + k_2 + k_c) \theta_{RS} + k_{-2} \underline{C}_P \theta_S C_{R,in} \quad (30)$$

$$\frac{d\theta_S}{dt} = -k_1 \underline{C}_R \theta_S C_{R,in} + (k_{-1} + k_2) \theta_{RS} - k_{-2} \underline{C}_P \theta_S C_{R,in} \quad (31)$$

2.3.3. Mechanism III

Mechanism III represents a more complicated case of coking where two surface species were involved. The rate expression is the same as in the previous cases, apart from reactions (5) and (6) whose rate equations are given below:

$$r_3 = k_3 \theta_{PS} \quad (32)$$

$$r_{-3} = k_{-3} \underline{C}_P \theta_S \quad (33)$$

$$r_{C2} = k_{C2} \theta_{PS} \quad (34)$$

The subsequent material balance for C_P , θ_{PS} , θ_S and θ_{CS} are stated below:

$$\frac{dC_P}{dt} = -\frac{C_P}{\varepsilon\tau} + \frac{k_3 \theta_{PS} \rho_{cat}}{C_{R,in}} - k_{-3} \underline{C}_P \theta_S \rho_{cat} \quad (35)$$

$$\frac{d\theta_{PS}}{dt} = k_2 \theta_{RS} + (k_3 - k_{C2}) \theta_{PS} + k_{-3} \underline{C}_P \theta_S C_{R,in} \quad (36)$$

$$\frac{d\theta_S}{dt} = -k_1 \underline{C}_R \theta_S C_{R,in} + k_{-1} \theta_{RS} + k_3 \theta_{PS} - k_{-3} \underline{C}_P \theta_S C_{R,in} \quad (37)$$

$$\frac{d\theta_{CS}}{dt} = k_C \theta_{RS} + k_{C2} \theta_{PS} \quad (38)$$

2.3.4. Mechanism IV

The rate expressions and material balance for mechanism IV are the same with mechanism III except for θ_{RS} and θ_{CS} which are given as follows:

$$r_{-c} = k_{-c} \theta_{CS} \quad (39)$$

$$\frac{d\theta_{RS}}{dt} = k_1 \underline{C}_R \theta_S C_{R,in} - (k_{-1} + k_2 + k_c) \theta_{RS} + k_{-c} \theta_{CS} \quad (40)$$

$$\frac{d\theta_{CS}}{dt} = k_C \theta_{RS} - k_{-c} \theta_{CS} \quad (41)$$

2.4. Kinetic Parameter Estimation Procedure

From its very inception, this work was intended to set up models for typical hydrocarbon catalytic reactions incorporating mechanisms of catalyst deactivation by coke formation. Arbitrary numerical values were assigned to the models associated parameters. Through a programmed numerical solution package, the model was able to calculate the time taken for coking reaction, i.e., the time for the catalyst activity to diminish and approach zero. The model had also demonstrated the effect of steps response of the modelling parameters on the rate of coking. Right and more appropriate values for modelling parameters could be obtained directly from experimental data or predicted from theoretical rules and available theories [23]. Therefore, a relevant catalytic reaction with all the corresponding parameter values was chosen from the literature as a case study. The reaction system is skeletal isomerisation of 1-pentene over a zeolite-based catalyst, as reported by Sandelin et al. [5]. They carried out parameter estimation using kinFit software as adopted from Aittamaa and Keskinen [24]. They compare their parameters estimation with experimental results for different coking deactivation models. The values used in this study (Table 1) are those that have good agreement with their experimental results. This reaction system was solely adopted for the purpose of obtaining kinetic parameters and obtaining a general understanding of catalyst deactivation phenomena.

Table 1. Input values for kinetic parameters.

$k, m^3s^{-1}kgcat^{-1}$	k_1	k_{-2}	k_{-3}	k_{-1}	k_2	k_3	k_c	k_{c2}	k_{-c}
Mechanism I	13	-	-	0.036	0.027	-	0.036	-	-
Mechanism II	13	1.349	-	0.036	0.027	-	0.036	-	-
Mechanism III	13	-	1.349	0.036	14.5	0.027	8.3×10^{-5}	4.6×10^{-8}	-
Mechanism IV	13	-	1.349	0.036	14.5	0.027	8.3×10^{-5}	-	4.6×10^{-8}

2.5. Numerical Method and Initial Conditions

The material balance equations derived in Sub-Section 2.3 are a series of ordinary differential equations (ODEs) consisting of several dependent variables with respect to a single independent variable, time (t). An array of numerical techniques can be used to simulate solutions for ODEs involving modelling of catalyst deactivation by coke deposition. However, MATLAB® was chosen as the programming language for this work due to its ability to successfully and directly illustrate matrix and array mathematics [25]. In particular, the ODE 45 solver is utilized due to its versatility as well as being employed for non-stiff differential equations [26]. The implementation of ODEs requires stating initial and boundary conditions of the reaction system of interest. The time (t) is set according to the time at which the system converges to steady state; therefore, the time boundary conditions in all experiments ranges from $t = 0$ to $t = 3 \times 10^5$ (s). The initial conditions at time (t) = 0 are set in accordance with the principle that active sites are not occupied by any species. The initial conditions of required parameters are set as follows:

$$\underline{C}_R = 1, \underline{C}_P = 0, \theta_{RS} = 0, \theta_{PS} = 0, \theta_{CS} = 0 \text{ and } \theta_S = 1$$

2.6. Sensitivity Analysis

Mathematical models are designed to mimic the reaction system, consequently validating reaction schemes and the nature of the reactions [27]. Local sensitivity measures are widely used in instances whereby differential equations are implemented and a better understanding of reaction paths and mechanisms are needed. Consequently, local sensitivity analysis is carried out for this study. Through stepwise parameter manipulations, simulations were carried out for Mechanisms I, II, III and IV. This consists of increasing or decreasing the magnitude of significant parameters ($k_1, k_{-1}, k_2, k_{-2}, k_3, k_{-3}, k_C, k_{C2}, k_{-C}, C_{R,in}, \rho_{cat}$ and τ) by a factor or percentage. While doing so, analyzing

cases where reaction rate constants are of equal magnitude facilitates the understanding of the impact each parameter has on the deactivation mechanism. This must therefore be implemented into the sensitivity studies.

3. Results and Discussion

The results are presented according to the mechanisms described in Sub-Section 3.3. For each mechanism, simulations were carried out using the parameter values reported in Tables 1 and 2, followed by sensitivity analysis. Since the objective here is to compare rival deactivation mechanisms, the sensitivity analysis was focused on the reaction rate constants. To avoid too many results, separate simulations were carried out and the results reported are those that showed higher sensitivity to coking.

Table 2. Additional parameters/variables.

Variable	Value
Residence time, τ (s)	1
Inlet reactant concentration, $C_{R,in}$ ($mol\ m^{-3}$)	20
Catalyst density, ρ_{cat} ($kg\ m^{-3}$)	600
Bed voidage, ε	0.4

3.1. Mechanism I

Figure 1 represents simulation results based on coking mechanism I and parameter values in Tables 1 and 2. As shown, at $t = 0$, the concentration of the reactant, C_R declined instantaneously, and then increased rapidly at $t = 20$ s. This is possible because at $t = 0$ s all the catalyst active sites are vacant allowing the reactant molecule to be strongly adsorbed into the free vacant sites. On the other hand, there is a steep rise in the concentration of θ_{RS} (adsorbed reactant) along with the product (C_P), both of which had reached a peak at $t = 20$ s. As the concentration of the free active sites decreases rapidly to zero, the conversion of C_R to θ_{RS} decreases proportionally with the decline in the C_P . The consumed θ_{RS} is mainly consumed to form coke (θ_{CS}) which increases continuously with time on stream.

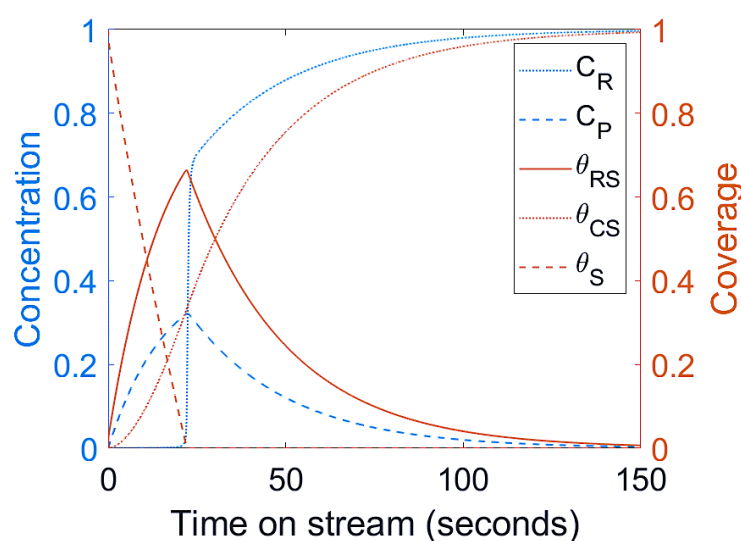


Figure 1. Estimated reactant and product concentration profiles (left axis) and surface species coverages (right axis) with respect to time for Mechanism I.

Sandelin et al. [5] carried out an integrated dynamic model for reaction kinetics and catalyst deactivation for skeletal isomerization of 1-pentene over ferrierite in a fixed bed

reactor. They have confirmed similar trends that when θ_{CS} approaches 1 after very long time on stream, the catalyst deactivates completely and is totally filled by coke. In line with this study, they found that θ_{RS} reaches maxima whereas θ_{CS} increases with increasing time on stream. Similarly, Lopez et al. [28] had observed higher deactivation of catalysts during 1-Pentene isomerization over SAPO-II, BEA, and AIMCM-41 molecular sieves at 250 °C, which was attributed to strong adsorption and higher coke formation. For the skeletal isomerization of n-alkenes over zeolite catalysts, it has been reported that the amount of Bronsted acid sites declines quite rapidly at the beginning of the experiment [28–32].

3.2. Mechanism II

Mechanism II has a reversible surface reaction, which distinguishes its deactivation mechanism from mechanism I. The reverse surface reaction is expected to produce more θ_{RS} and part of this will participate in coking reaction, hence more coke would be formed. If more coke is formed, then the deactivation in mechanism II would be severe. Comparison of Figure 1 for mechanism I with Figure 2 for mechanism II reveals no difference in coke formation and products deactivation. The only clear difference in mechanism II (Figure 2) is that it produced more θ_{RS} and less C_P as expected but the extent of deactivation after long time on stream is the same as shown in Figure 2. Coke formation is always extreme and rapid process within the first few seconds of time on stream [33–39]. The main deactivation occurred on the strongest acid sites at a short time on stream. As shown in Figure 3, the process of coke formation in mechanism I and II had been pictured in more details at a few seconds of time on stream. Based on the result, the deactivation in mechanism II had occurred earlier with more coke deposition compared to mechanism I. The modelling results and the reaction kinetics were in good agreement.

The introduction of the reverse surface reaction in mechanism II resulted in the production of extra θ_{RS} which facilitated higher coke production and earlier deactivation of the products. Therefore, when coke is formed from adsorbed surface reactant, reversibility of the surface reaction enhances the coke formation and induces earlier deactivation of the catalyst.

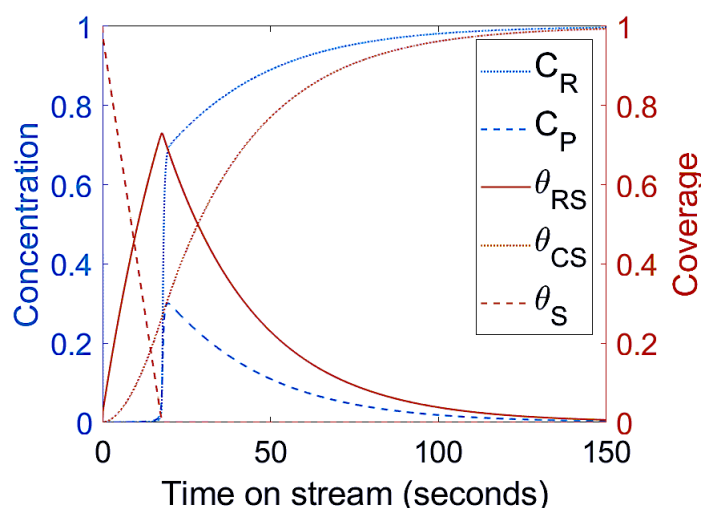


Figure 2. Estimated reactant and product concentration profiles (left axis) and surface species coverages (right axis) with respect to time for Mechanism II.

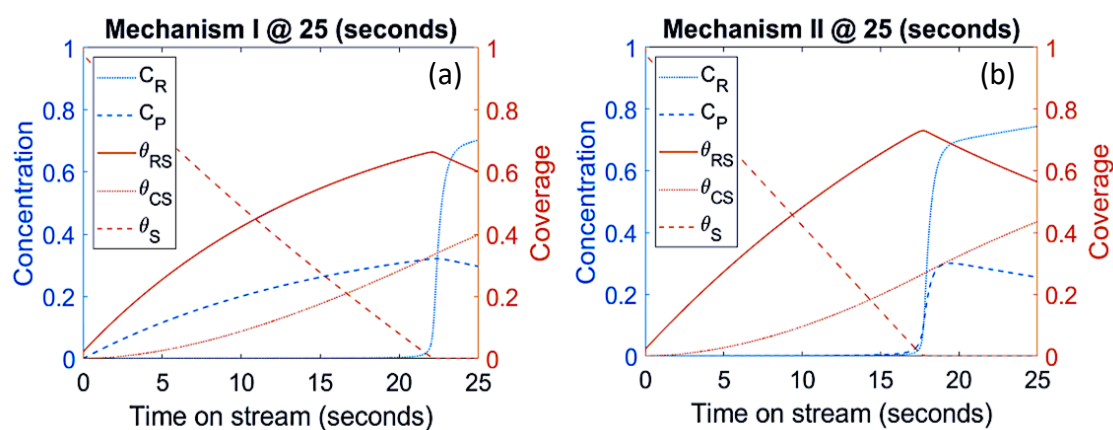


Figure 3. Estimated reactant and product concentration profiles (left axis) and surface species coverages (right axis) with respect to time: comparison between mechanism I (Fig. 3a) and mechanism II (Fig. 3b).

3.3. Mechanism III

Mechanism III as stated earlier contained two surface species or coke precursors participating in coke formation. The consequence of the catalyst deactivation depends on the net rate constant of each surface species. As provided in Table 1, the input values for the coking rate constants corresponding to the mechanism III are very small and therefore negligible coke is deposited on the catalyst. Seeing at the far right of Figure 4, for mechanism III, the production of coke can be detected after very long time on stream, approximately 28 h. As shown in Figure 4, the amount of θ_{RS} produced with time on stream is very low due to its rapid consumption to produce θ_{PS} , while on the other hand, θ_{PS} had reached its maximum coverage within a few seconds of time on stream. Coke is favorably formed from θ_{PS} due to its higher production and low consumption by other competing steps. For both surface species to be active in coke formation there must be a balance in their production and consumption rates. In Figure 4, θ_{PS} acted as the main coke precursor due to its abundance on the active sites of the catalyst. Even though the adsorbed intermediates θ_{RS} and θ_{PS} individually react further to produce coke, the rate at which θ_{RS} desorb to form θ_{PS} determines their individual strength on the coke formation and catalyst deactivation. If the rate of desorption is high, then θ_{PS} would be the main coke precursor and if the rate is low, θ_{RS} would be the major coke precursor.

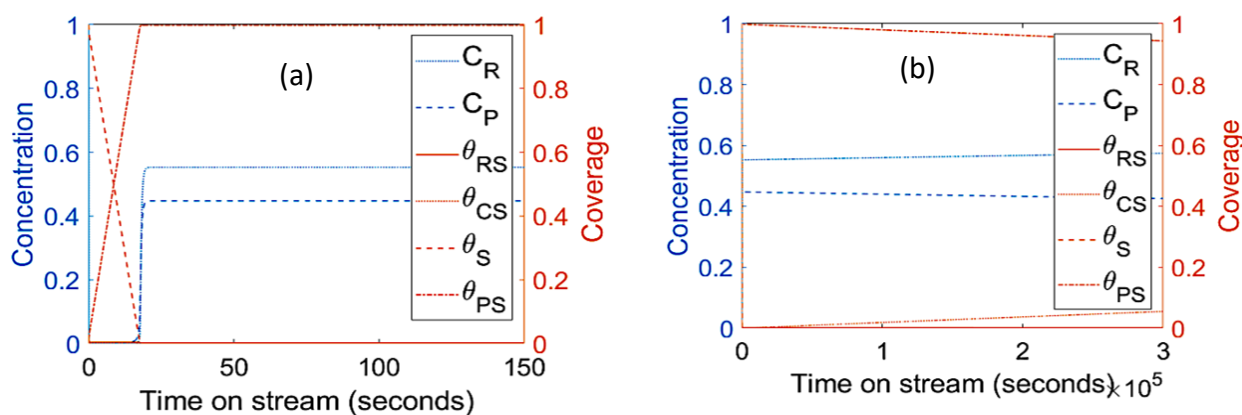


Figure 4. Estimated reactant and product concentration profiles (left axis) and surface species coverages (right axis) with respect to time for mechanism III at different scales of time on stream: a) Short times on stream up to 150 s. b) Large times on stream.

3.4. Mechanism IV

As stated earlier, the presence of reversible coke formation distinguishes mechanism IV from III. The coke formed on the catalyst is very low and noticed only after very long time on stream. Based on the modelling results presented in Figure 4, the deactivation mechanisms III and IV are unique and only relevant at higher coking rates. In order to study the effect of this reversible deactivation mechanism, the coking rate constants need to be manipulated so that significant coking took place in the system. This was implemented through the sensitivity analysis of mechanism IV.

3.5. Sensitivity Analysis

3.5.1. Mechanisms I and II: Sensitivity to k_1 , k_{-1} , k_2 , k_c and τ

For mechanism I, sensitivity analysis was carried out for all the elementary reaction steps and the results are presented in Figure 5. As shown in Figure 5a when k_1 receives high values, then θ_S will decrease rapidly. This is also in agreement with Equations (14), (15) and (23), respectively. In Figure 5a, k_1 was reduced by 100% and k_{-1} was increased by 10%. As expected, since k_1 receives lower value compared to k_{-1} , the adsorption of

the reactant (R) on the active sites was very slow, which means that it takes longer time for all the available active sites to be occupied. As shown in Figure 5a θ_S approaches zero at $t = 100$ s, i.e., almost five times slower than in Figure 1. Based on this deactivation mechanism, coke (θ_{CS}) is mainly formed from the adsorbed reactant (θ_{RS}) and when k_1 is lower than k_{-1} then lower amounts of θ_{RS} and C_p are obtained; hence, the coke formation is slower. For instance, in Figure 1, the coke coverage reaches 0.7 within 50 s whereas slower deactivation was obtained in Figure 5a where θ_{CS} fractional coverage reaches 0.55 within the same 50 s. The increase in the concentration of the free vacant acid sites when the feed desorbs to a greater extent than adsorbs was also reported by Sandelin et al. [5].

Figure 5b considers the sensitivity by changing k_2 whose value determines the level of the product (C_p). As k_2 had been increased by 10%, slower and constant coking is obtained with lower amount of θ_{RS} due to its increased consumption in the product desorption step. The rate of coking here is slow and constant, and it takes 300 s for all the active sites to be occupied by coke molecules. This type of coke is a result of further transformation of coke precursors. The volatile coke molecules as well as heavy coke molecules can either undergo cracking to yield smaller molecules, which are desorbed or react via dehydrogenation leading to more condensed coke species [1]. These findings are in line with the kinetic expression in Equation (2), as the increase of k_2 is expected to increase both the product formation as well as the fraction of vacant active sites. The coke content had decreased at higher desorption rate of the coke precursors responsible for coke formation [33].

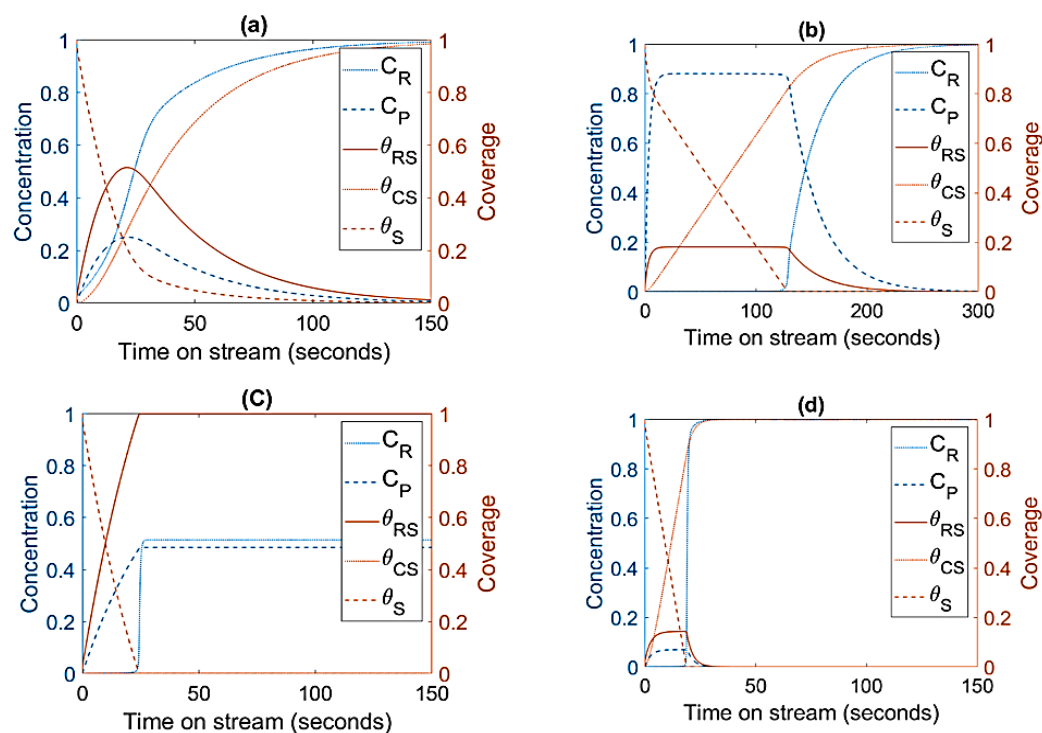


Figure 5. Estimated reactant and product concentration profiles (**left y-axis**) and surface species coverages (**right y-axis**) with respect to time: sensitivity analysis for Mechanism I, (a) with reduced k_1 by 100% and increased k_{-1} by 10% (b) increased k_2 by 10% (c) $k_C = 0.36$ (d) $\tau = 5$ s.

In Figure 5c, increasing k_C by 10% leads to significantly higher coke formation and early deactivation of θ_{RS} and C_P . It takes almost 150 s for all the active sites to be filled and occupied by coke in Figure 1, but when k_C was increased by 10% (Figure 5c), the catalyst active sites are totally filled by coke and became completely deactivated within 25 s of time on stream. Therefore, k_C should be kept as small as possible to obtain appreciable amount of the products. The rate of formation of coke evidently occurs at a much faster rate with increasing k_C ; however, the decline of active sites remains unaffected. The lack of variation of the active sites with respect to changing magnitudes of k_C suggests the competitive inhibition is occurring between θ_{RS} and θ_{CS} . This phenomenon favorably confirms to the findings from Beeckman and Froment [34] and further supports the concept that the main and coking reaction occur by a single mechanism on the same active sites [34]. This has also confirmed that the decline in the concentration of θ_{RS} and C_P is due to the deactivation of the catalyst by the coke deposition [5,21].

As shown in Figure 5d, the larger the residence time, τ , the greater the bonding of the reactant to the active sites, as a result more product and less coke are formed. Theoretically, more coke should be deposited at higher residence times as it favors the secondary cracking reactions leading to high coke formation [35]. As presented in Figures 1 and 5d, respectively, higher conversion and lower coke content are obtained at higher residence times. This finding was supported by Brillis and Manos [33,36] and Zhang et al. [37]. Onay et al. [38] reported that high residence times were able to keep the conversion level considerably higher and presented a much slower apparent activity decline. The effect of coke formation with varying residence time is a complicated issue arising from the complication of the coking process. From their deactivation studies during catalytic cracking of C_8 aliphatic hydrocarbons over ultrastable Y zeolite, Brillis and Manos [36] reported that the high residence time runs could present a falsified picture of deactivation. Supported by results from the literature, a better explanation can be made that validates the effect of coke formation at varying residence time. The catalyst deactivates rapidly due to

the fast initial formation of coke on strong zeolitic acid sites [31–33, 36]. However, the formation of coke from smaller precursors on weaker acid sites is much slower and significantly slows down the deactivation process [31–33]. Coke precursors formed initially at short residence times are very volatile, and they are further desorbed into gas phase products or transformed into condensed hard coke at higher residence time [31,32]. The higher amount of products obtained at higher residence time are due to the slower coking process leading to a lower declined in catalyst activity.

3.5.2. Mechanisms II: Sensitivity to k_2 , k_{-2} , and τ

The sensitivity analysis for Mechanism II was restricted to the surface reaction elementary step, as it is the basic step that differentiates the deactivation mechanism II from I. The behavior of coke is always expected to change with residence time, so residence time was also included as part of the sensitivity analysis.

As shown in Figure 6a, k_2 was increased by 100% whereas k_{-2} is decreased by 10%, similar with the sensitivity analysis of mechanism I in the adsorption step. The results of these changes are very clear. The enhanced consumption of θ_{RS} to produce the product has lowered the coke deposition and generally slowed down the deactivation. As seen in Figure 2, the full deactivation had occurred around 150 s whereas in Figure 6a the active sites are fully occupied by coke at around 250 s. Hence, speeding the product formation step has lowered the coke formation and reduced the severity of the deactivation on the catalyst.

The next sensitivity analysis for mechanism II deals with adjustment of residence time. As shown in Figure 6b, increasing the residence time, τ , increases the bonding of the reactant to the active sites. As a result, more product and less coke are formed. Even though the effect of residence time is general, the mechanism through which coke is formed determines the time and extent of the deactivation. At all the residence times simulated, coke formation is more detrimental in mechanism II compared to mechanism I. For similar deactivation mechanisms, the deactivation behaviors are similar and quite indistinguishable at low residence time and higher amount of inlet concentration due to the rapid formation of coke on strong acidic sites of the catalyst.

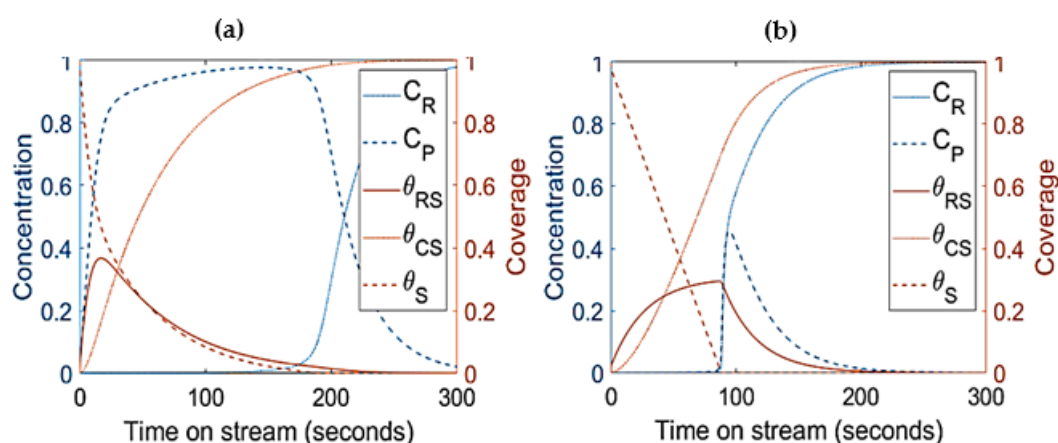


Figure 6. Estimated reactant and product concentration profiles (left axis) and surface species coverages (right axis) with respect to time: sensitivity analysis for Mechanism II, (a) with increased k_2 by 100% and (b) decreased k_{-2} by 10% ($\tau = 5$ s).

3.5.3. Mechanisms III: Sensitivity to k_c and k_{c2}

Separate simulations and preliminary results showed that k_c and k_{c2} are the most important parameters that influence the coke formation for mechanism III. As shown in Figure 7a, if k_c is increased by 10^5 while k_{c2} remain unchanged, θ_{RS} will suddenly decline with heavy coke formation. The full deactivation of the product was attained around 500 s of time on stream. The coking tendency could also be enhanced by increasing the magnitude of k_{c2} as shown in Figure 7b. Since k_{c2} is smaller compared to k_c , when both are increased by the same factor, the coke formation with k_{c2} is slower with full deactivation around 1000 s of time on stream (Figure 7b). When the coking is slower, more θ_{RS} and C_P are formed, signifying slow deactivation of the products.

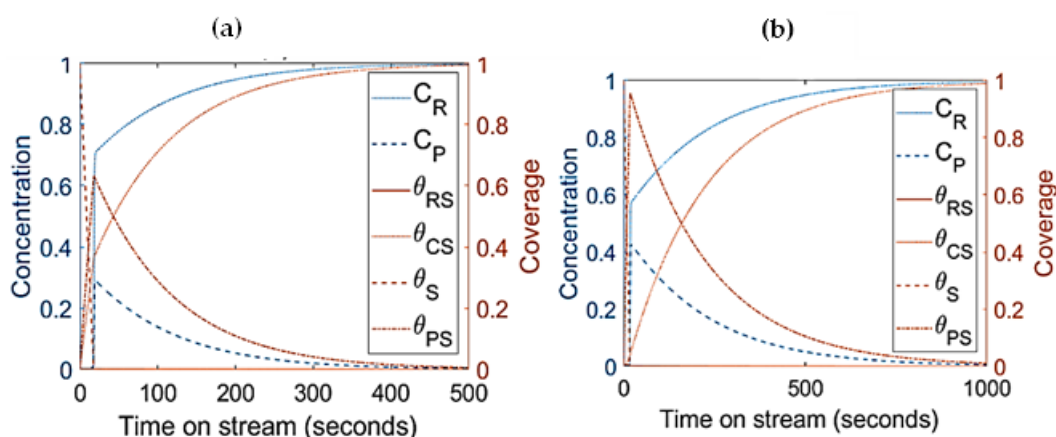


Figure 7. Estimated reactant and product concentration profiles (left axis) and surface species coverages (right axis) with respect to time: sensitivity analysis for Mechanism III, (a) with increased k_c by 10^5 and k_{c2} unchanged (b) with increased k_{c2} by 10^5 and k_c unchanged.

Generally, for two surface species deactivation mechanism, increasing the rate constant of one of the coking steps would certainly increase the deactivation of the system and reduce the activity of the catalyst. Although all the deactivation models provided reasonable description of coke formation, modelling results and experimental work from Sandelin et al. [21] showed that better results were typically obtained by assuming θ_{RS} reacting to form coke. This is reasonable because in the beginning, the concentration of θ_{RS} is high and the deactivation is fast, and thus the fit is better for θ_{RS} as a coke precursor. Both θ_{RS} and θ_{PS} can represent the coke precursor and reacted to form coke especially at low concentrations [5].

3.5.4. Mechanisms IV: Sensitivity to k_c and k_{c2}

Separate simulations had showed that the similarities between mechanism III and IV had cut across all the parameters, making their sensitivity analysis very similar. Decreasing k_c by 10^{-5} produced the similar results for both mechanism III and IV, respectively. In both cases, significant coking took place with the available active sites fully occupied by coke in around 500 s. Due to its higher rate of production, θ_{PS} represents the most available surface species and widely affected coke formation. On the other hand, changing k_{-c} by 10^{-5} (Figure 8b) further retarded the coke formation compared to the elementary model (Figure 8a), and this is due to the reversibility of coking mechanism.

As shown by separate simulations, when k_{-c} was changed by 10^{-5} , coke was not deposited up to 83 h, whereas for the elementary model (Figure 8a), coke was deposited after 28 h. In most catalytic reactions, catalyst maintains residual activity after a long time-

on-stream, which can be explained by self-regeneration caused by reversible coking deactivation mechanism [21]. Modelling of coke formation using reversible deactivation kinetics was reported to fit the experimental data very well [21].

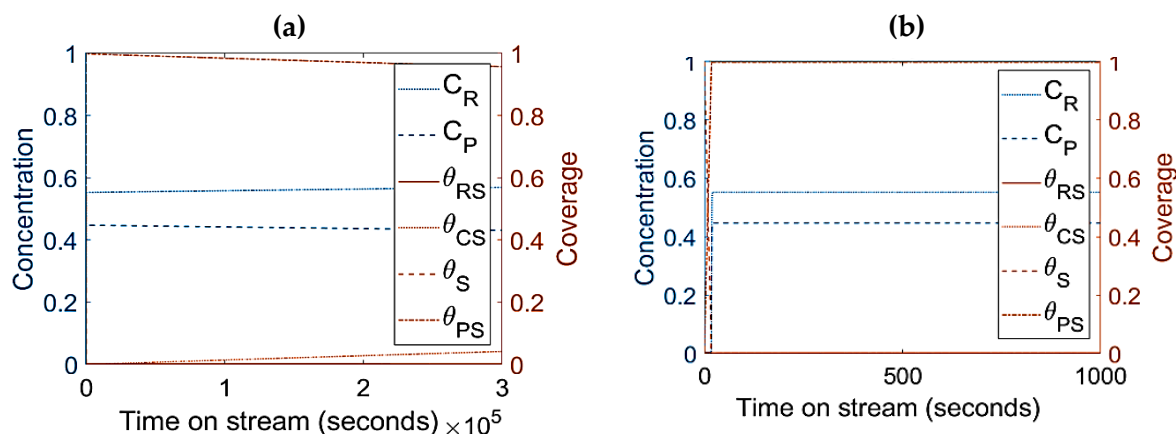


Figure 8. Estimated reactant and product concentration profiles (left axis) and surface species coverages (right axis) with respect to time: sensitivity analysis for Mechanism IV, (a) elementary model, using parameters values in Tables I and II (b) with decreased k_{-c} by 10^{-5} and k_c unchanged.

3.6. Model Verifications

The mathematical model was verified by comparing the modelling results with related work from literature sources. For the sake of validation, the following experimental findings were used.

- One of the major findings of this work is that increasing the inlet reactant concentration increases the coke formation in all mechanisms, as the adsorbed reactant concentration contributes to coke formation (as shown in separate simulations). This is supported by experimental results by Föttinger et al. [40]. They conducted skeletal isomerization of 1-pentene on BEA zeolite and on ferrierite (FER). From their findings with increasing partial pressure of 1-pentene the conversion decreases, and coke formation increase. This agrees with thermodynamic consideration, which suggested that higher alkene partial pressure could favor dimerization and hydride transfer reactions. Sandelin et al. [5,21] carried out dynamic Modelling of Catalyst Deactivation for the skeletal-isomerization of 1-Pentene on Ferrierite. They revealed that increasing of the feed olefin partial pressure increases the coke formation.
- Modelling work from Salmi et al. [41] showed that catalyst deactivation can be suppressed by adding more catalyst to the system. In agreement with the latter results, simulations from present work as shown in Figure 9 had similar behaviors where the increasing catalyst density suppresses the coke formation. The available active sites and product concentration increases with increasing catalyst density while the production of θ_{RS} is suppressed. Even though the deactivation is delayed with increasing catalyst density, there is a limit at which further addition of catalyst does not accomplish higher conversion. Similar findings were reported by Manos et al. [42] and Gulab et al. [43] where, at low reaction temperatures, the addition of extra catalyst above polymer-to-catalyst mass ratios of 2 does not enhance conversion. As shown in Figure 9, increasing the catalyst density up to 75% has improved the conversion but at 100% increment and above, the conversion remained the same. Among the important feature here is the stabilization of the products at higher concentration of catalyst due to the low coke. As shown by separate simulations, increasing the catalyst density by 400% does not improve the conversion, but it has increased the stability of product production and further lowered coke formation.

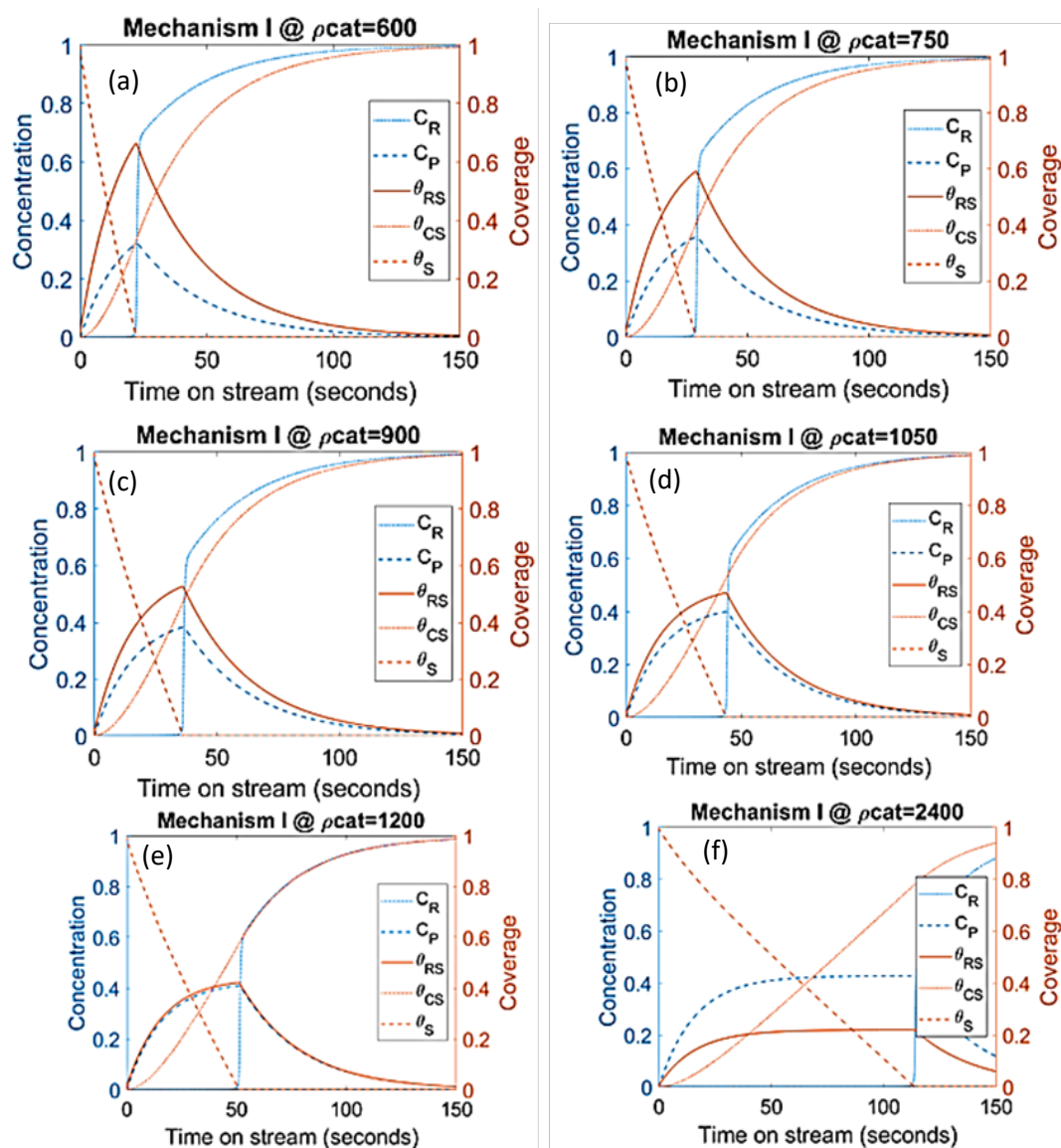


Figure 9. Estimated reactant and product concentration profiles (left axis) and surface species coverages (right axis) with respect to time: showing the effect of increasing catalyst amount. a: $\rho_{cat}=600$ g cm⁻³. b: $\rho_{cat}=750$ g cm⁻³. c: $\rho_{cat}=900$ g cm⁻³. d: $\rho_{cat}=1050$ g cm⁻³. e: $\rho_{cat}=1200$ g cm⁻³. f: $\rho_{cat}=2400$ g cm⁻³.

- The parameters/variables values used for this modelling work were generated from the work of Sandelin et al. [4]. Their work is basically based on plug flow reactor whereas the present modelling is based on CSTR. The same principal shapes and types of step responses can be observed in both reactor types, CSTR and a plug flow

reactor (PFR) [44]. The qualitative behavior of CSTR was reported to be very similar to this of PFR [44,45]. Surface species coverages were compared between PFR (the literature) and CSTR (present study) as part of the modelling validation (Figure 10). The same parameters/variables values were used in both cases. As shown in Figure 10, the principal shapes and types of steps responses are the same in CSTR and PFR confirming the validity of the CSTR modelling. In the two reactors, the coverage of n-pentene (A) rises rapidly from zero to a maximum value, and then starts to decline as the coverage of coke (C) increases with increasing time on stream. If k_1 is decreased and k_{-1} is increased, the free vacant sites increase, especially in the beginning of the experiment. This trend can easily be seen for PFR (Figure 10c,d). When small changes occur, the responses in CSTR (as shown in Figure 10a,b) are less pronounced due to back mixing effects [44]. However, if k_1 decreases up to a higher value (as shown in Figure 5a), the step responses can be more noticeable, similar to those observed in PFR. The differences observed are expected and are reported in similar comparison studies.

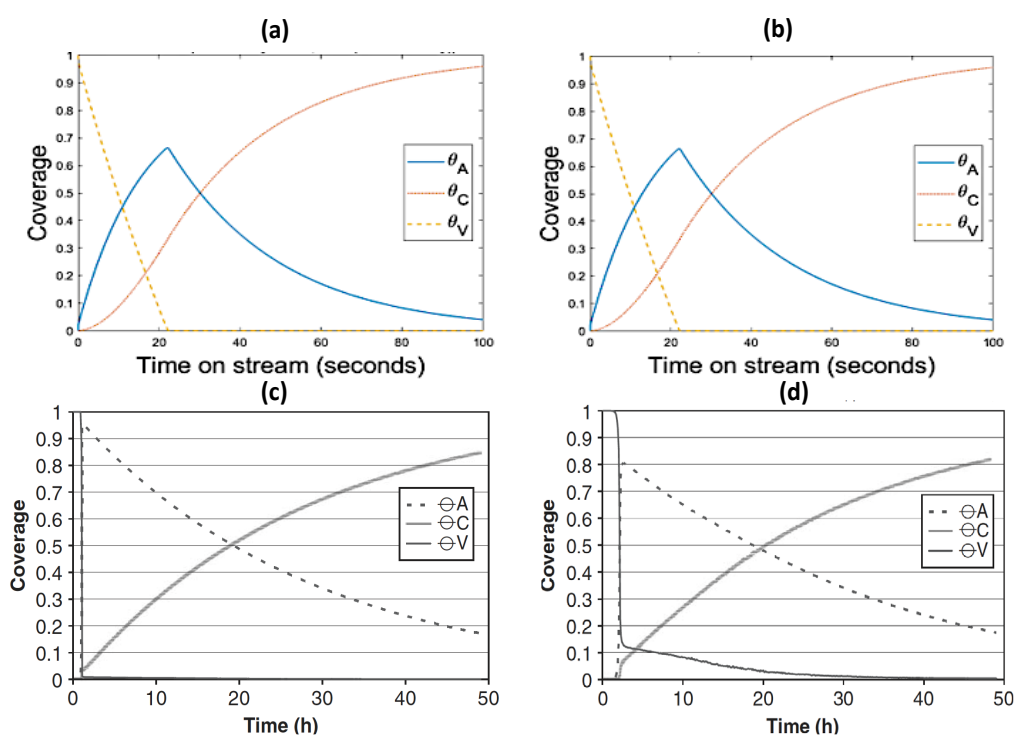


Figure 10. Estimated surface compound coverages: Comparison between CSTR (present study) and PFR (literature study), (a) mechanism I (elementary model, CSTR), (b) mechanism I (reduced k_1 by 20% and increased k_{-1} by 10%, CSTR), (c) literature (elementary model, PFR), (d) literature (reduced k_1 by 20% and increased k_{-1} by 10%, PFR).

Lercher et al. [45] studied the comparative deactivation of H-ZSM-5 catalyst during testing in PFR and CSTR reactors. The two reactors had similar product distribution, but the catalyst deactivation rates differ significantly due to the different local concentration in the two reactors, which is similar to the present study. Figure 10 shows that in the CSTR, changes in the concentration of surface species occurred immediately with time on stream, whereas in the PFR reactor, a gap was observed. Lercher et al. [45] reported a similar scenario, where an initial phase with no conversion was observed at very short contact times in the PFR, while conversion started immediately at short contact times in the CSTR, without an initiation zone. This is attributed to the excellent mixing condition and homogeneous distribution of reaction products in the CSTR [45].

4. Conclusions

Catalyst deactivation by coking was modelled in a simple, robust, and efficient approach. The approach is useful for various kinds of reactors. A similar model approach when compared with experimental results is suggested to be useful for process scale-up and is safer than an empirical deactivation model. This modelling approach has a general significance since the modelled reaction system can represent numerous hydrocarbon transformations. The methodology developed utilizing ODE 45 on MATLAB, producing 2-dimensional plots, facilitated a greater understanding on the impact of reaction parameters on the nature of the reaction. The shape of the response is very much determined by the magnitude of kinetic parameters and the inlet concentration of the reactants. The modeling results showed that the mechanisms were most sensitive to the inlet concentration, while the inhibition of the active site, with respect to the adsorbed molecules, had the greatest influence on the time scale of deactivation. Furthermore, the coke formation rate is higher at higher rate of adsorption, leading to very fast deactivation. At lower residence times and higher inlet concentrations, the formation of coke is very rapid, whereas at higher residence times, product formation is higher with lower coke formed. The more reversible the surface reaction is, the more the coke formation is enhanced inducing earlier deactivation of the catalyst. For the reversible deactivation mechanism, the catalyst maintains residual activity after prolong time on stream. Comparative analysis with the literature revealed that the model is indeed able to successfully demonstrate the most essential features of catalyst deactivation and is therefore useful for process scale-up purposes. Future work is aimed to extend the study to different reactors such as a plug flow reactor.

Author Contributions: Conceptualization, I.M. and G.M.; Methodology, I.M. and N.M.; Software, I.M.; Validation and Analysis, I.M., D.Z., N.M. and T.G.A.; Writing—original draft preparation, I.M.; Writing—review and editing, G.M., D.Z., N.M. and T.G.A.; Funding acquisition, Petroleum Technology Development Fund (PTDF). All authors have read and agreed to the published version of the manuscript.

Funding: A PhD studentship sponsored by Petroleum Technology Development Fund (PTDF), a subsidiary of Nigeria National Petroleum Co-operation (NNPC).

 **Institutional Review Board Statement:**

Informed Consent Statement:

Data Availability Statement: The data presented in this study are available on request from the first author (IM).

Acknowledgments: First author (IM) gratefully acknowledges Petroleum Technology Development Fund (PTDF), a subsidiary of Nigeria National Petroleum Co-operation (NNPC), for sponsoring his PhD study.

Conflicts of Interest: The authors declare no conflict of interest.

References

1. Chen, S.; Manos, G. Study of Coke and Coke Precursors during Catalytic Cracking of n-Hexane and 1-Hexene over Ultrastable Y Zeolite. *Catal. Lett.* **2004**, *96*, 195–200. <https://doi.org/10.1023/B:CATL.0000030120.29538.5d>.
2. Chen, S.; Manos, G. In situ thermogravimetric study of coke formation during catalytic cracking of normal hexane and 1-hexene over ultrastable Y zeolite. *J. Catal.* **2004**, *226*, 343–350. <https://doi.org/10.1016/j.jcat.2004.06.004>.
3. Froment, G.F. Modeling of catalyst deactivation. *Appl. Catal. A Gen.* **2001**, *212*, 117–128.
4. Nam, I.S.; Kitrell, J.R. Use of Catalyst Coke Content in Deactivation Modeling. *Ind. Eng. Chem. Process Des. Dev.* **1984**, *23*, 237–242. <https://doi.org/10.1021/i200025a008>.
5. Sandelin, F.; Salmi, T.; Murzin, D.Y. An integrated dynamic model for reaction kinetics and catalyst deactivation in fixed bed reactors: Skeletal isomerization of 1-pentene over ferrierite. *Chem. Eng. Sci.* **2006**, *61*, 1157–1166. <https://doi.org/10.1016/j.ces.2005.08.018>.
6. Sie, S.T. Consequences of catalyst deactivation for process design and operation. *Appl. Catal. A* **2001**, *212*, 129–151.
7. Szepe, S.; Levenspiel, O. *Proceedings of the Fourth European Symposium on Chemical Reaction Engineering*; Pergamon Press: Brussels, Belgium, 1971; p. 265.

8. Quintana-Solórzano, R.; Thybaut, J.W.; Marin, G.B.; Lødeng, R.; Holmen, A. Single-Event Microkinetics for coke formation in catalytic cracking. *Catal. Today* **2005**, *107–108*, 619–629. <https://doi.org/10.1016/j.cattod.2005.07.036>.
9. Reyniers, M.F.; Beirnaert, H.; Marin, G.B. Influence of coke formation on the conversion of hydrocarbons: I. Alkanes on a USY-zeolite. *Appl. Catal. A* **2000**, *202*, 49–63.
10. Chen, Z.; Zhang, X.; Yang, F.; Peng, H.; Zhang, X.; Zhu, S.; Che, L. Deactivation of a Y-zeolite based catalyst with coke evolution during the catalytic pyrolysis of polyethylene for fuel oil. *Appl. Catal. A Gen.* **2021**, *609*, 117873. <https://doi.org/10.1016/j.apcata.2020.117873>.
11. Chen, Z.; Zhang, X.; Che, L.; Peng, H.; Zhu, S.; Yang, F.; Zhang, X. Effect of volatile reactions on oil production and composition in thermal and catalytic pyrolysis of polyethylene. *Fuel* **2020**, *271*, 117308. <https://doi.org/10.1016/j.fuel.2020.117308>.
12. Seifert, M.; Jonscher, C.; Haufe, L.A.; Weigand, J.J. Deactivation kinetics of ZSM-5 by coke in Ethanol-to-Hydrocarbons process. *Chem. Ing. Technol.* **2021**, *93*, 747–753. <https://doi.org/10.1002/cite.202000228>.
13. Nazarova, G.Y.; Ivashkina, E.N.; Ivanchina, E.D.; Vosmerikov, A.V.; Vosmerikova, L.N.; Antonov, A.V. A model of catalytic cracking: Product distribution and catalyst deactivation depending on saturates, aromatics and resins content in feed. *Catalysts* **2021**, *11*, 701. <https://doi.org/10.3390/catal11060701>.
14. Moustafa, T.M.; Corella, J.; Froment, G.F. Kinetic modeling of coke formation and deactivation in the catalytic cracking of vacuum gas oil. *Ind. Eng. Chem. Res.* **2003**, *42*, 14–25. <https://doi.org/10.1021/ie0204538>.
15. John, Y.M.; Patel, R.; Mujtaba, I.M. Maximization of propylene in an industrial FCC unit. *Appl. Petrochem. Res.* **2018**, *8*, 79–95.
16. Alonso-Ramírez, G.; Cuevas-García, R.; Sánchez-Minero, F.; Ramírez, J.; Moreno-Montiel, M.; Silva-Oliver, G.; Ancheyta, J. Catalytic hydrocracking of a Mexican heavy oil on a MoS₂/Al₂O₃ catalyst: II. Study of the transformation of isolated aromatics fraction obtained from SARA analysis. *Fuel* **2021**, *288*, 119541.
17. Al-Khattaf, S.; Saeed, M.R.; Aitani, A.; Klein, M.T. Catalytic Cracking of Light Crude Oil to Light Olefins and Naphtha over E-Cat and MFI: Microactivity Test versus Advanced Cracking Evaluation and the Effect of High Reaction Temperature. *Energy Fuels* **2018**, *32*, 6189–6199.
18. Radu, S.; Ciuparu, D. Modelling and Simulation of an Industrial Fluid Catalytic Cracking. *Rev. Chim.-Ducharest-Orig.* **2014**, *65*, 113–119.
19. Hinshelwood, C.N. *The Kinetics of Chemical Change*; Clarendon Press: Oxford, UK, 1940; Chapter 8.
20. Hougen, O.A.; Watson, R.M. *Chemical Process Principles*; Part III; Wiley: New York, NY, USA, 1959; Chapter 19.
21. Sandelin, F.; Salmi, T.; Murzin, D.Y. Dynamic Modeling of Catalyst Deactivation in Fixed-Bed Reactors: Skeletal Isomerization of 1-Pentene on Ferrierite. *Ind. Eng. Chem. Res.* **2006**, *45*, 558–566. <https://doi.org/10.1021/ie050550b>.
22. Jalid, F.; Haider, M.A.; Alam, M.I.; Khan, T.S. Mechanistic insights into the dominant reaction route and catalyst deactivation in biogas reforming using ab initio microkinetic modelling. *Catal. Sci. Technol.*, **2021**, *11*, 2130–2143. <https://doi.org/10.1039/d0cy02155e>.
23. Shahrouzi, J.R.; Guillaume, D.; Rouchon, P.; Da Costa, P. Stochastic Simulation and Single Events Kinetic Modeling: Application to Olefin Oligomerization. *Ind. Eng. Chem. Res.* **2008**, *47*, 4308–4431. <https://doi.org/10.1021/ie071215l>.
24. Aittamaa, J.; Keskinen, K. *Kinfit User's Instruction Manual*; Neste Engineering: Porvoo Finland/HUT: Espoo, Finland, 2003.
25. 7 Reasons Matlab Is the Easiest and Most Productive Environment for Engineers and Scientists. 2017. Available online: <https://uk.mathworks.com/products/matlab/why-matlab.html> (accessed on 15 March 2023).
26. Ode45. 2017. Available online: <https://uk.mathworks.com/help/matlab/ref/ode45.html> (accessed on 15 March 2023).
27. Saltelli, A.; Ratto, M.; Tarantola, S.; Campolongo, F. Sensitivity analysis for chemical models. *Chem. Rev.* **2005**, *105*, 2811–2828. <https://doi.org/10.1021/cr040659d>.
28. Lopez, C.M.; Ramirez, L.; Sazo, V.; Escobar, V. 1-Pentene isomerization over SAPO-II, BEA and AIMCM-41 molecular sieves. *Appl. Catal. A Gen.* **2008**, *340*, 1–6.
29. Van Donk, S.; Bus, E.; Broersma, A.; Bitter, J.H.; de Jong, K.P. Butene skeletal isomerization over H-ferrierite: A TEOM and in situ IR study on the role of carbonaceous deposits and the location of Bronsted acid sites. *Appl. Catal. A* **2002**, *237*, 149–159.
30. Vahteristo, K.; Sahala, K.M.; Laari, A.; Solonen, A.; Haario, H. Skeletal isomerization kinetics of 1-pentene over an HZSM-22 catalyst. *Chem. Eng. Sci.* **2010**, *65*, 4640–4651. <https://doi.org/10.1016/j.ces.2010.05.008>.
31. Wang, B.; Manos, G. Acid Site Characterization of Coked USHY Zeolite Using Temperature Programmed Desorption with a Component-Nonspecific Detector. *Ind. Eng. Chem. Res.* **2007**, *46*, 7977–7983. <https://doi.org/10.1021/ie0708733>.
32. Wang, B.; Manos, G. Role of Strong Zeolitic Acid Sites on Hydrocarbon Reactions. *Ind. Eng. Chem. Res.* **2008**, *47*, 2948–2955. <https://doi.org/10.1021/ie071353a>.
33. Brillis, A.A.; Manos, G. Coke Formation during Catalytic Cracking Of C₈ Aliphatic Hydrocarbons Over Ultrastable Y Zeolite. *Ind. Eng. Chem. Res.* **2003**, *42*, 2292–2298. <https://doi.org/10.1021/ie020460w>.
34. Beeckman, J.W.; Froment, G.F. Catalyst deactivation by site coverage and pore blockage. *Chem. Eng. Sci.* **1980**, *35*, 805–815. [https://doi.org/10.1016/0009-2509\(80\)85064-0](https://doi.org/10.1016/0009-2509(80)85064-0).
35. Serrano, D.P.; Aguado, J.; Escola, J.M.; Garagorri, E. Conversion of low density polyethylene into petrochemical feedstocks using a continuous screw kiln reactor. *J. Anal. Appl. Pyrolysis* **2001**, *58–59*, 789–801. [https://doi.org/10.1016/S0165-2370\(00\)00153-4](https://doi.org/10.1016/S0165-2370(00)00153-4).
36. Brillis, A.A.; Manos, G. Deactivation studies during catalytic cracking of C₈ aliphatic hydrocarbons over ultrastable Y-zeolite. Conversion and product yield profiles with time onstream. *Catal. Lett.* **2003**, *91*, 185–191. <https://doi.org/10.1023/B:CATL.0000007153.29038.32>.

37. Zhang, X.; Lei, H.; Yadavalli, G.; Zhu, L.; Wei, Y.; Liu, Y. Gasoline-range hydrocarbons produced from microwave-induced pyrolysis of low-density polyethylene over ZSM-5. *Fuel* **2015**, *144*, 33–42. <https://doi.org/10.1002/9783527684403.ch3>.
38. Onay, O.; Beis, S.H.; Koçkar, O.M. Fast pyrolysis of rape seed in a well-swept fixed-bed reactor. *J. Anal. Appl. Pyrol.* **2001**, 58–59, 995–1007. [https://doi.org/10.1016/S0165-2370\(00\)00133-9](https://doi.org/10.1016/S0165-2370(00)00133-9).
39. Wang, B.; Manos, G. A novel thermogravimetric method for coke precursor characterization. *J. Catal.* **2007**, *250*, 121–127. <https://doi.org/10.1016/j.jcat.2007.05.018>.
40. Föttinger, K.; Kinger, G.; Vinek, H. 1-pentene isomerization over FER and BEA. *Appl. Catal. A Gen.* **2003**, *249*, 205–212. [https://doi.org/10.1016/S0926-860X\(03\)00192-3](https://doi.org/10.1016/S0926-860X(03)00192-3).
41. Salmi, T.; Murzin, D.Y.; Wärnä, I.; Mäki-Arvela, P.; Martin, G. Integrated modelling of reaction and catalyst deactivation kinetics—Hydrogenation of sitosterol to sitostanol over a palladium catalyst. *Chem. Eng. Sci.* **2013**, *104*, 156–165. <https://doi.org/10.1016/j.ces.2013.09.003>.
42. Manos, G.; Garforth, A.; Dwyer, J. Catalytic Degradation of high density polyethylene on an ultrastable Y zeolite. nature of initial polymer reactions, pattern of formation of gas and liquid products, temperature effects. *Ind. Eng. Chem. Res.* **2000**, *39*, 1198–1203.
43. Gulab, H.; Jan, M.R.; Shah, J.; Manos, G. Plastic catalytic pyrolysis to fuels as tertiary polymer recycling method: Effect of process conditions. *J. Environ. Sci. Health Part A* **2010**, *45*, 908–915. <https://doi.org/10.1080/10934521003709206>.
44. Salmi, T. Modelling and Simulation of Transient States of Ideal Heterogeneous Catalytic Reactors. *Chem. Eng. Sci.* **1988**, *43*, 503–551.
45. Sun, X.Y.; Mueller, S.; Liu, Y.; Shi, H.; Haller, G.L.; Sanchez-Sanchez, M.; Van Veen, A.C.; Lercher, J.A. Coke formation and deactivation pathways on H-ZSM-5 in the conversion of methanol to olefins. *J. Catal.* **2015**, *325*, 48–59. <https://doi.org/10.1016/j.jcat.2015.02.013>.

Disclaimer/Publisher's Note: The statements, opinions and data contained in all publications are solely those of the individual author(s) and contributor(s) and not of MDPI and/or the editor(s). MDPI and/or the editor(s) disclaim responsibility for any injury to people or property resulting from any ideas, methods, instructions or products referred to in the content.